MASTER

CONSIDERATIONS IN MEASURING TRACE RADIONUCLIDES IN SOIL SAMPLES BY L X-RAY DETECTION

CONF-771023--20

M. G. Strauss, I. S. Sherman, E. J. Swanson, R. H. Pehl

Prepared for

IEEE Nuclear Science Symposium
San Francisco, CA
October 19-21, 1977

NOTICE

This report was prepared as an account of work sponsored by the United States Government. Neither the United States nor the United States Department of Energy, nor any of their employees, nor any of their contractors, subcontractors, or their employees, makes any warranty, express or implied, or assumes any legal liability or responsibility for the accuracy, completeness or usefulness of any information, apparatus, product or process disclosed, or represents that its use would not infringe privately owned rights.

DISTRIBUTION OF THIS DOCUMENT IS UNLIMITED

ARGONNE NATIONAL LABORATORY, ARGONNE, ILLINOIS

UofC-AUA-USERDA

operated under contract W-31-109-Eng-38 for the
U. S. ENERGY RESEARCH AND DEVELOPMENT ADMINISTRATION

The facilities of Argonne National Laboratory are owned by the United States Government. Under the terms of a contract (W-31-109-Eng-38) between the U. S. Energy Research and Development Administration, Argonne Universities Association and The University of Chicago, the University employs the staff and operates the Laboratory in accordance with policies and programs formulated, approved and reviewed by the Association.

MEMBERS OF ARGONNE UNIVERSITIES ASSOCIATION

The University of Arizona	Kansas State University	The Ohio State University
Carnegie-Mellon University	The University of Kansas	Ohio University
Case Western Reserve University	Loyola University	The Pennsylvania State University
The University of Chicago	Marquette University	Purdue University
University of Cincinnati	Michigan State University	Saint Louis University
Illinois Institute of Technology	The University of Michigan	Southern Illinois University
University of Illinois	University of Minnesota	The University of Texas at Austin
Indiana University	University of Missouri	Washington University
Iowa State University	Northwestern University	Wayne State University
The University of Iowa	University of Notre Dame	The University of Wisconsin

NOTICE

This report was prepared as an account of work sponsored by the United States Government. Neither the United States nor the United States Energy Research and Development Administration, nor any of their employees, nor any of their contractors, subcontractors, or their employees, makes any warranty, express or implied, or assumes any legal liability or responsibility for the accuracy, completeness or usefulness of any information, apparatus, product or process disclosed, or represents that its use would not infringe privately-owned rights. Mention of commercial products, their manufacturers, or their suppliers in this publication does not imply or connote approval or disapproval of the product by Argonne National Laboratory or the U. S. Energy Research and Development Administration.

Presented at the Nuclear Science Symposium, October 19-21, 1977 San Francisco, California.
To be published in the IEEE Trans. Nucl. Sci. NS-25, No. 1, February 1978.

CONSIDERATIONS IN MEASURING TRACE RADIONUCLIDES IN SOIL SAMPLES BY L X-RAY DETECTION*

M. G. Strauss, I. S. Sherman, E. J. Swanson
Argonne National Laboratory, Argonne, Illinois 60439

and

R. H. Pehl
Lawrence Berkeley Laboratory, Berkeley, California 99720

ABSTRACT

Several aspects pertaining to the measurements of trace radionuclides (such as plutonium) in soil samples by L x-ray detection have been considered. A 3 x 3 multiplexed array of edge-mounted Si detectors with a total detection area of 50 cm^2 and FWHM resolution of 300 eV at 17 keV has been conceived. The fractional transmission-weighted solid angle for a distributed, self-absorbing source was calculated to be 0.25, which is one half the value of that for a lossless sheet source. To determine the minimum detectable activity, intensities of 59 L x-ray lines from the decay chains of ^{238}U and ^{232}Th have been calculated. A total of 130 x rays ranging from 9-20 keV emanate from soil per 100 alpha decays each of ^{232}Th and ^{238}U, compared with 4.6 for ^{239}Pu. The minimum Pu activity detectable with the Si array in such contaminants as worldwide fallout, weapons material, and Rocky Flats soil is expected to approach 1 pCi in 1 g of soil. This concentration is comparable to the natural activity in soil. The minimum Pu activity detectable with NaI detectors is 100 times higher.

I. Introduction

The growing desire to measure radioactive contamination in the environment has stimulated interest in new measurement techniques. Presently nearly all sensitive laboratory methods involve the concentration of the radioactive elements by chemical separation followed by α spectroscopy. Although capable of measuring very low concentrations, these procedures are difficult, laborious and therefore costly. Direct photon spectroscopy without prior chemical processing of the sample is simpler, more amenable to routine measurements, and likely to be less costly. When gamma emission from the radionuclide of interest is weak or interference obscures significant portions of it, as in the case of plutonium, measurement by x-ray detection may be more effective. High resolution x-ray spectrometry can also serve as an effective method complementary to in-situ radiation monitoring. The distribution of radioactivity in the soil depth must be known in order to make meaningful in-situ estimates of activity concentration. This depth profile changes from one geographical location to another as well as with time and weather. Measurements of x rays from soil samples taken from different depths, in conjunction with conventional field measurements, could provide more complete and accurate information about the distribution and concentration of radioactivity in soil.

We explored the feasibility of measuring by L x-ray detection contaminant activity concentrations on the order of 1 pCi in 1 g of soil, comparable to the natural activity of ^{232}Th and ^{238}U in soil. A low background Si detector system suitable for soil sample measurements was conceived. To determine the expected count yield in the detector the transmission-weighted solid angle subtended about a distributed, self-absorbing source was evaluated. The minimum detectable activity is expected to be limited in many cases by line interference from the natural radiation in soil. We therefore have analyzed the transitions in the decay chains of ^{232}Th and ^{238}U in soil and calculated the intensities of all the significant L x-ray lines associated with each deexcitation. Finally, the expected detection sensitivity for several radioactive contaminants, such as fallout and reactor waste, was evaluated for a Si array and compared with NaI detectors.

II. Detector

We have conceived a Si detector array in which each crystal is mounted on its edge and has a thin window on both sides. This edge-mounting geometry doubles the detection area and permits the placement of a NaI detector on each side of the Si detector array.

*Work performed under the auspices of the U. S. Energy Research and Development Administration.

Figure 1 shows this configuration for the prototype Si detector currently under development. The detector is attached to and insulated from the cold rod with a boron nitride (BN) mount. Soil samples are sandwiched between the NaI crystals and the corresponding face of the Si detector.

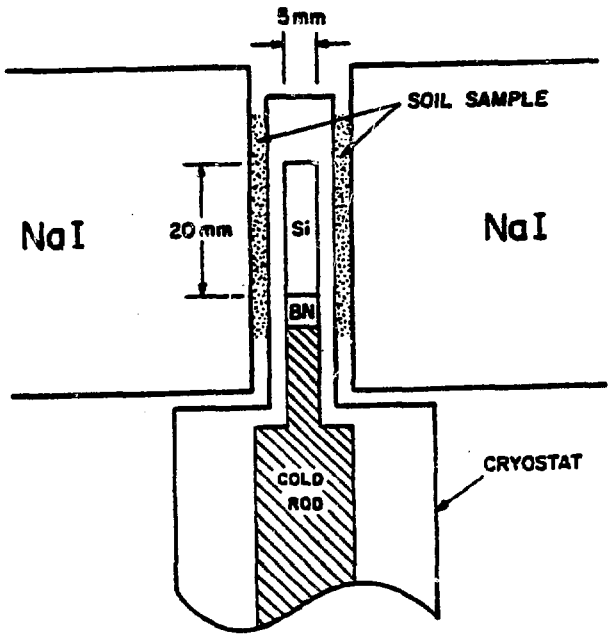

Fig. 1 Configuration of Si x-ray detector for soil sample measurements. Si crystal is mounted on edge to double detection area. NaI detectors in anticoincidence with Si detector suppress background continuum.

Gamma radiation from ^{40}K and ^{137}Cs in the soil or from shield penetration that scatters in the Si detector will contribute to the background unless suppressed. Since such events will largely be also detected in one of the NaI detectors, they are readily rejected.

The energy resolution needed for this system is governed by two conflicting requirements. On the one hand, the resolution should be adequately high to separate the spectral lines of interest from background interference and from each other. On the other hand, to obtain an adequate number of counts a large detector area is needed, which inevitably results in high detector capacitance. The latter is of course in direct conflict with high resolution. On the basis of preliminary measurements and evaluation of the expected background, we arrived at a reasonable compromise consisting of a detector having an area of 300 mm^2, a thickness of 5 mm, and a FWHM resolution of 300 eV at 17 keV.

The system being considered for routine measurements of contaminant radionuclides in soil samples is shown in Fig. 2. It consists of a 3 x 3 detector array with dimensions shown in Fig. 1 so as to yield a total detection area of about 50 cm^2. Individual amplifying channels multiplexed into a common multichannel analyzer will essentially maintain the 300 eV resolution of a single detector. A 15 cm diameter NaI

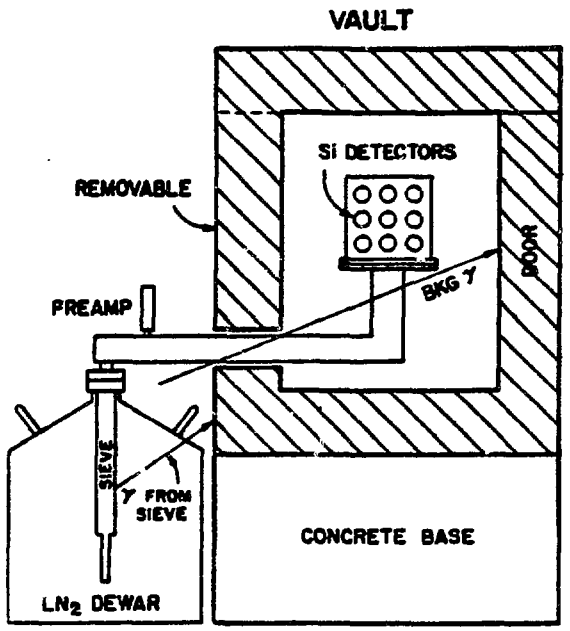

Fig. 2 Si detector array for soil sample measurements. Detectors are mounted in configuration of Fig. 1 inside shielded vault. Liquid nitrogen dewar is placed outside vault to shield detector from molecular sieve radiation and to permit filling without disturbing measurements.

crystal (not shown) will face each side of the detector array. The cryostat head will be situated in a vault so as to prevent background radiation leakage from intercepting the detectors. Placing the liquid nitrogen dewar outside the vault shields the detectors from radiation emanating from the molecular sieve and permits filling the dewar without having to disturb long measurements.

III. Solid Angle

The solid angle determines the fraction of the radiation incident on a detector from a point in a radioactive sample. In the case of a lossless sheet source adjacent to the detector this fraction is 0.5 corresponding to the solid angle 2π subtended by the detector about an elemental area in the source. Thus, the radiation intensity incident on the detector is

$$I = \Omega \cdot I_o = 0.5\, I_o \qquad (1)$$

where I_o is the radiation per unit area solid angle emanating from the sheet source in both directions and Ω is the geometric solid angle (fractional).

In the case of a distributed source like a soil sample, the fraction of the radiation incident on a detector is reduced due to absorption in the soil matrix. For a soil sample of infinite thickness and area the radiation intensity I_a per unit area of the source intercepting the detector was calculated (Appendix A) to be

$$I_a = 0.25\, I_n \qquad (2)$$

where I_n is the radiation per unit area solid angle normal to the surface of the sample. Thus, for the case where $I_n = I_o$, the fraction of the detected

radiation from a distributed self-absorbing source is one half of that from a sheet source. The difference is due to the additional attenuation in the absorber resulting from the longer path length in the off-axis direction relative to the normal direction.

Equation (2) can be interpreted in terms of solid angle by stating it as

$$I_a = \Omega_T I_n = 0.25\, I_n \qquad (3)$$

where Ω_T is equal to the geometric solid angle Ω weighted by a transmission factor T due to the additional attenuation in the off-axis direction. Thus

$$\Omega_T = T \cdot \Omega = 0.25 \qquad (4)$$

where $T = 0.5$ and $\Omega = 0.5$

Much insight into the variations of radiation intensity with sample thickness and angle of incidence can be obtained from a graphical analysis. An infinitely thick sample was hypothetically divided into five layers of progressively increasing thickness such that each layer contributed 1/5 of the total normal intensity I_n at the detector. Each layer was then represented by an equivalent point source. The intensity per unit area solid angle $dI/d\Omega$ and the solid angle Ω were calculated as a function of the angle θ (with respect to the normal) as outlined in Appendix A. Plots of $dI/d\Omega$ vs. Ω for layers I, III, and V are shown in Fig. 3. The radiation intensity I_i at the surface of the sample contributed by the i^{th} layer is then equal to the area under the i^{th} curve:

$$I_i = \int_0^{0.5} \frac{dI_i}{d\Omega}\, d\Omega \,. \qquad (5)$$

The total intensity I_a from all five layers is obtained by graphically summing the individual layer contributions:

$$I_a = \sum_{i=1}^{5} I_i = 0.25\, I_n. \qquad (6)$$

This is the same result as that obtained analytically in Appendix A.

The effect of off-axis attenuation as a function of sample thickness can also be seen in Fig. 3. The thickness of each layer was chosen so as to give equal normal intensity at the surface of $0.2\, I_n$. For radiation in the off-axis direction the path length increases with angle and therefore results in additional attenuation. Layer I, near the surface, is thin and therefore does not introduce much additional attenuation. Hence, the curve is rather square looking with a cutoff at $\Omega = 0.5$ similar to that of a sheet source. As the sample thickness increases, the additional off-axis attenuation decreases the intensity at large angles. This is reflected in the change of the shape of the curves and their cutoffs. Curve III is not square but nearly a triangle with a cutoff at $\Omega \approx 0.4$ and curve V is concave rather than convex with a cutoff at $\Omega \approx 0.3$.

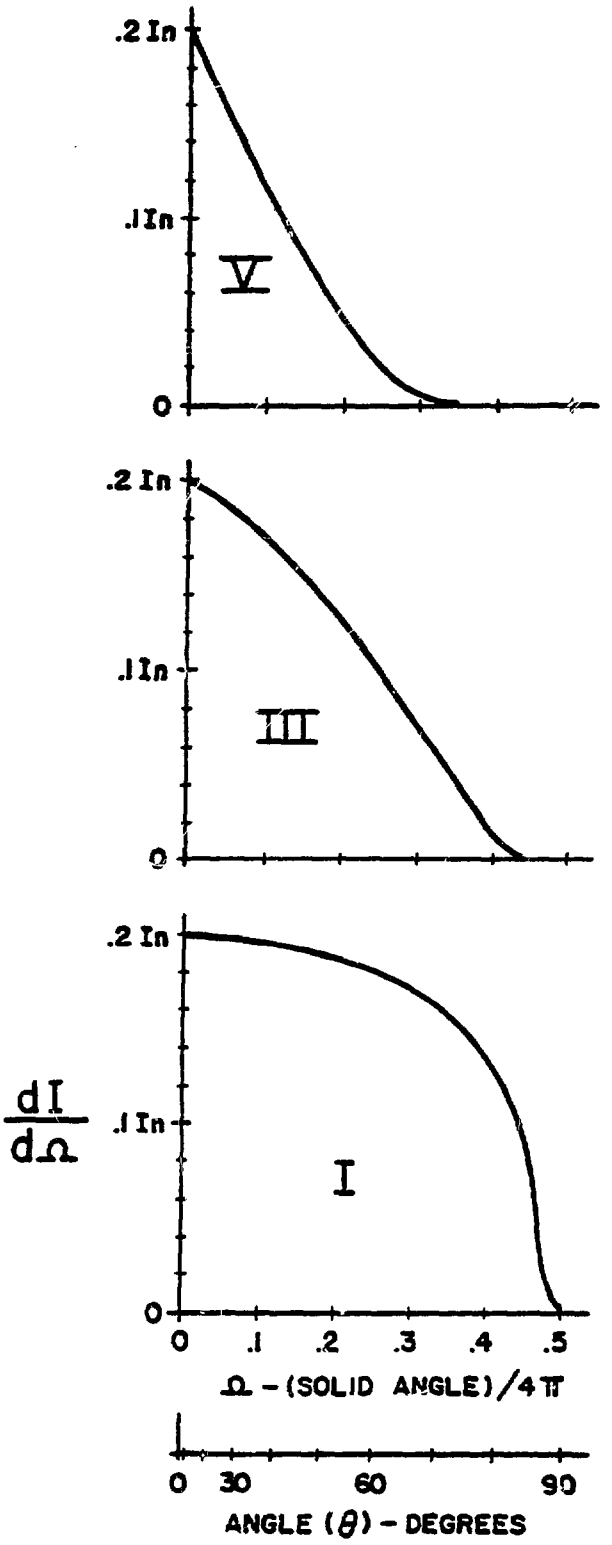

Fig. 3 Variation of radiation intensity with angle of photon path for three layers of increasing thickness of a planar, infinitely thick, distributed source. Layer I is at surface, layer III is intermediate, and layer V is at far end. Note decrease in intensity at large angles as layer thickness increases from I to V.

The radiation intensity vs. sample thickness is the progressive sum of the layer contributions as shown in Fig. 4. The contribution of the first layer is

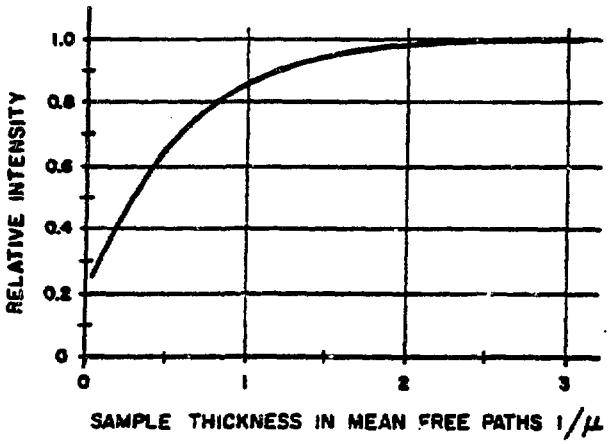

Fig. 4 Variation of radiation intensity with thickness of distributed source. Essentially all available radiation can be obtained from a source thickness of two mean free paths.

plotted vs. the distance from the surface to the point source representing this layer. The sum contribution of the first and second layers is plotted against the distance of the point source representing the second layer, etc. It is readily seen that essentially all the available radiation can be obtained from a sample whose thickness is two mean free paths. For the case of Pu, the mean free path of UL_γ x rays (20 keV) in soil is about 2.5 mm. Hence, the sample thickness need not exceed 5 mm.

In order to avoid a reduction in radiation intensity at the detector edge, the sample diameter should exceed the diameter of the detector. If it does not, radiation from the edge of the sample in a direction away from the detector is not compensated for by radiation into the detector. In the case where the sample is adjacent to the detector, the extension beyond the detector edge need only be as long as the sample thickness for essentially full compensation.

IV. Count Yield

The expression for the expected count yield in the detector is derived from Eq. (3). Consider a differential layer of thickness dx cm and density ρ g/cm^3 having a specific activity of a disintegrations per min (dpm) per g which produces I_x photons per disintegration. The photon intensity per unit solid angle from this layer is $a I_x \rho dx$ photons/cm^2/min. The differential intensity in the normal direction dI_n that would be observed from this layer through an absorber of given thickness x cm, having a linear attenuation coefficient μ cm^{-1} would be

$$dI_n = a I_x \rho e^{-\mu x} dx. \qquad (7)$$

If the activity were distributed throughout an absorber of thickness d cm, the total normal intensity per unit area solid angle is

$$I_n = a I_x \rho \int_0^d e^{-\mu x} dx = \frac{a I_x}{\mu/\rho}\left(1 - e^{-\mu d}\right). \qquad (8)$$

For an infinitely thick absorber ($d = \infty$)

$$I_n = \frac{a I_x}{\mu/\rho} \quad \text{photons/cm}^2\text{/min} \qquad (9)$$

where μ/ρ is the mass attenuation coefficient in cm^2/g.

From Eqs. (3) and (9) the intensity per unit area solid angle from a distributed planar source of infinite thickness is

$$I_a = \Omega_T I_n = \Omega_T \frac{a I_x}{\mu/\rho} \qquad (10)$$

where $\Omega_T = 0.25$ is the transmission-weighted solid angle. For a detector having an Area A cm^2 and a peak efficiency η at the energy of interest, the detector count yield is

$$N = 0.25 \frac{a I_x}{\mu/\rho} A \cdot \eta \quad \text{counts/min.} \qquad (11)$$

V. Background X Rays

The background radiation is normally the major factor in determining the minimum detectable level of a contaminant radionuclide. The use of the NaI detectors in anticoincidence with the Si detector is expected to keep the background continuum below the peaks of the x rays emitted in the decay chains of natural ^{238}U and ^{232}Th in soil. Thus, the minimum detectable level is likely to be limited by line interference of the background x rays with the x-ray peaks of interest. In order to determine the degree of interference and subsequently the minimum detectable level, we calculated the intensities of the L x rays in the above decay chains.

The decay of ^{238}U and ^{232}Th produces daughter products, some of which are in excited states. The deexcitation of these nuclei is predominantly by internal conversion which is accompanied by the emission of L x rays. We have calculated the intensity of these x rays, assuming equilibrium conditions exist between parent nuclides and all daughter products except for radon. For that case, it was assumed[1] that 8% of the gas escapes from the soil and thereby correspondingly reduces the x-ray intensities from ^{222}Rn daughters.

The total L x-ray intensity is the product of the L electron conversion intensity and the average L shell fluorescent yield. The conversion intensity was obtained from the internal conversion coefficient e/γ and either the branching intensity or the gamma intensity. Values for these quantities were taken from compilations, using experimental values when given, in preference to theoretical values. Table I lists the calculated intensities of the total L x rays emitted in soil from the decay chains of ^{238}U and ^{232}Th. Intensities less than 0.05 are indicated by a dash.

Table I

INTENSITIES OF L X RAYS EMANATING FROM SOIL
IN THE DECAY CHAINS OF ^{238}U AND ^{232}Th

^{238}U Decay Chain	L X Rays per 100 α Decays of ^{238}U (by Transition Multipolarity)	^{232}Th Decay Chain	L X Rays per 100 α Decays of ^{232}Th (by Transition Multipolarity)
$^{238}U \rightarrow {}^{234}Th + \alpha$	9.1 (E2)	$^{232}Th \rightarrow {}^{228}Ra + \alpha$	8.4 (E2)
$^{234}Th \rightarrow {}^{234m}Pa + \beta^-$	11.6 (1.12 E1, 3.29 E2, 7.18 M1)	$^{228}Ra \rightarrow {}^{228}Ac + \beta^-$	---
		$^{228}Ac \rightarrow {}^{228}Th + \beta^-$	29.1 (E2)
$^{234m}Pa \rightarrow {}^{234}U + \beta^-$	0.4 (E2)	$^{228}Th \rightarrow {}^{224}Ra + \alpha$	9.8 (E2)
$^{234}U \rightarrow {}^{230}Th + \alpha$	11.0 (E2)	$^{224}Ra \rightarrow {}^{220}Rn + \alpha$	0.3 (E2)
$^{230}Th \rightarrow {}^{226}Ra + \alpha$	8.7 (E2)	$^{220}Rn \rightarrow {}^{216}Po + \alpha$	---
$^{226}Ra \rightarrow {}^{222}Rn + \alpha$	0.4 (E2)	$^{216}Po \rightarrow {}^{212}Pb + \alpha$	---
$^{222}Rn \rightarrow {}^{218}Po + \alpha$	---	$^{212}Pb \rightarrow {}^{212}Bi + \beta^-$	2.5 (M1)
$^{218}Po \rightarrow {}^{214}Pb + \alpha$	---	α Bi branch (36%):	
$^{214}Pb \rightarrow {}^{214}Bi + \beta^-$	5.6* (M1)	$^{212}Bi \rightarrow {}^{208}Tl + \alpha$	8.7 (M1)
$^{214}Bi \rightarrow {}^{214}Po + \beta^-$	0.1* (E2)	$^{208}Tl \rightarrow {}^{208}Pb + \beta^-$	0.1 (0.04 E2, 0.06 M1)
$^{214}Po \rightarrow {}^{210}Pb + \alpha$	---	β Bi branch (64%):	
$^{210}Pb \rightarrow {}^{210}Bi + \beta^-$	24.7* (M1)	$^{212}Bi \rightarrow {}^{212}Po + \beta^-$	---
$^{210}Bi \rightarrow {}^{210}Po + \beta^-$	---	$^{212}Po \rightarrow {}^{208}Pb + \alpha$	---
$^{210}Po \rightarrow {}^{206}Pb + \alpha$	---		

*8% escape of ^{222}Rn from soil was assumed.

For high resolution x-ray analysis the intensity of the constituent lines (L_{α_1}, L_{β_1}, etc.), which make up the totals (Table I) are of critical importance. A given L x ray is characterized by a unique transition from a particular subshell in a higher shell to a given L subshell. Thus, an L_{β_1} x ray is emitted when a vacancy in subshell II of shell L is filled by an electron from subshell IV in shell M. The intensity with which a given x ray is emitted is equal to the product of the number of radiative transitions to the L subshell and the emission rate resulting from filling a vacancy in a given L subshell by an electron from a particular subshell in a higher shell. The number of radiative transitions is a function of the subshell fluorescent yield and of the primary vacancies produced by internal conversion following radioactive decay and modified by intrashell Coster-Kronig radiationless transitions. The distribution of primary vacancies in the subshells is a function of the transition multipolarity and energy. Hence, the relative intensities of the various L x-ray lines is different when produced as a result of an E1, E2 or M1 transition. An outline of the procedure used in calculating the x-ray intensities is given in Appendix B.

The calculated line intensities produced in each of the decays listed in Table I are given in Appendix C. Summing for each line the intensity contributions from all the decays gives the total intensity for each x ray (Table II) emanating from soil per 100 decays of ^{238}U and 100 decays of ^{232}Th.

As a test of the calculation procedure we computed the intensities of the UL x rays emitted in the decay of ^{238}Pu and ^{239}Pu and the NpL x rays emitted in the decay of ^{241}Am and compared them (Table III) with values obtained by several experimenters. The columns designated ΣL_{α_1}, ΣL_{β_1} and ΣL_{γ_1} denote peak complexes which in the calculations correspond to the sum of the most intense L_{α_1}, L_{β_1} and L_{γ_1} x rays. The calculated x-ray intensities are seen to be within the range of the measured values. We therefore expect comparable accuracy to apply to Tables I and II and assume that these calculated intensities provide meaningful information for estimating background interference.

Table II

LINE INTENSITIES OF L X RAYS EMANATING FROM SOIL IN THE DECAY CHAINS OF ^{238}U AND ^{232}Th

Energy (keV)	X-Ray Line	Intensity†	Energy (keV)	X-Ray Line	Intensity†
8.55	TlL_{ℓ}	0.2	14.63	TlL_{γ_2}	0.1
9.42	BiL_{ℓ}	0.8	14.73	TlL_{γ_3}	0.2
10.17	TlL_{α_2}	0.4	14.76	RaL_{β_4}	0.1
10.27	TlL_{α_1}	3.4	14.84	RaL_{β_2}	1.7
10.63	RaL_{ℓ}	0.6	15.23	RaL_{β_1}	11.0
10.73	BiL_{α_2}	1.5	15.24	BiL_{γ_1}	1.3
10.84	BiL_{α_1}	13.0	15.39	RaL_{β_5}	0.3
11.12	ThL_{ℓ}	1.0	15.55	RaL_{β_3}	0.1
11.35	PaL_{ℓ}	0.3	15.58	BiL_{γ_2}	0.5
11.72	RnL_{α_1}	0.2	15.62	ThL_{β_2}	3.2
11.93	TlL_{β_4}	0.6	15.64	ThL_{β_4}	0.1
12.19	RaL_{α_2}	0.6	15.71	BiL_{γ_3}	0.5
12.21	TlL_{β_1}	1.7	16.02	PaL_{β_2}	0.8
12.27	TlL_{β_2}	0.7	16.10	PaL_{β_4}	1.0
12.34	RaL_{α_1}	8.4	16.20	ThL_{β_1}	20.1
12.39	TlL_{β_3}	0.6	16.21	ThL_{β_5}	0.6
12.64	TlL_{β_5}	0.1	16.43	ThL_{β_3}	0.1
12.69	BiL_{β_4}	2.1	16.63	PaL_{β_5}	0.2
12.81	ThL_{α_2}	1.7	16.70	PaL_{β_1}	2.5
12.97	ThL_{α_1}	15.3	16.77	RnL_{γ_1}	0.1
12.98	BiL_{β_2}	2.5	16.93	PaL_{β_3}	0.9
13.02	BiL_{β_1}	6.3	17.22	UL_{β_1}	0.2
13.12	PaL_{α_2}	0.4	17.84	RaL_{γ_1}	2.4
13.21	BiL_{β_3}	2.4	18.42	RaL_{γ_6}	0.5
13.29	PaL_{α_1}	3.8	18.98	ThL_{γ_1}	4.5
13.39	BiL_{β_5}	0.3	19.56	PaL_{γ_1}	0.6
13.61	UL_{α_1}	0.1	19.60	ThL_{γ_6}	0.8
14.29	TlL_{γ_1}	0.3	19.90	PaL_{γ_2}	0.3
14.31	RnL_{β_1}	0.3	20.09	PaL_{γ_3}	0.3
			20.22	PaL_{γ_6}	0.1

†X rays per 100 ^{238}U α decays and 100 ^{232}Th α decays.

Table III

CALCULATED INTENSITIES OF L X RAYS COMPARED WITH EXPERIMENTAL VALUES

Source of Data	X Rays/100 α Decays				
	ΣL	L_ℓ	ΣL_{α_1}	ΣL_{β_1}	ΣL_{γ_1}
$^{238}Pu \rightarrow {}^{234}U + \alpha$					
This calculation	11.4		4.17	5.91	1.31
Vasilik et al[2]	13.9		5.05	7.41	1.48
Swinth[3]	11.4				
Halley et al[4]	10.6				
Byrne et al[5]	12.9				
$^{239}Pu \rightarrow {}^{235}U + \alpha$					
This calculation	4.7		1.72	2.42	0.54
Newton[6]	4.6		1.67	2.38	0.55
Swinth[3]	4.6				
Coddington[7]	4.6				
Ahmad[8]	6.7				
Israel[9]	2.9				
West et al[10]	4				
$^{241}Am \rightarrow {}^{237}Np + \alpha$					
This calculation	35.7	0.86	14.27	16.85	3.71
Campbell et al[11]	38.2	0.86	13.2	19.25	4.85
IAEA[12]	37.7	0.8	13.5	18.4	5.0
Gehrke et al[13]	37.3	0.81	12.6	19.1	4.75

VI. Minimum Detectable Pu Activity

The minimum detectable activity of a radionuclide in soil can be estimated by evaluating the peaks of interest, in this case due to Pu, relative to the background and and other interference lines. The background is assumed to consist primarily of L x-ray interference peaks produced in the decay chains of ^{232}Th and ^{238}U in soil whose calculated intensities are listed in Table II. Virtually all Pu mixtures also contain some ^{241}Am. The decay of ^{241}Am produces NpL x-ray peaks which also interfere with the UL x rays from Pu. The degree of interference depends on the abundance of ^{241}Am relative to Pu. The line intensities of U and NpL x rays have been calculated (Table IV) using measured values[2,3,11] for the total L x-ray intensities. Table IV also lists calculated intensities of U and NpL x rays from weapons material, Rocky Flats soil, worldwide fallout, and reactor waste material (aged 10 yrs), all of which are of interest in environmental measurements. The intensities of the mixtures are based on estimates of their isotopic composition.[14]

The expected detector count rates for each of the above contaminants and for soil background have been calculated from Tables IV and II and Eq. (11) and are presented in Figs. 5-7 in the form of bar-type diagrams. The peaks of interest are represented by triangles in which the height is proportional to the count rate and the base is equal to 2 x FWHM = 0.6 keV. Lines that are separated by 0.3 keV (FWHM) or less and are not expected to be fully resolved have been combined into a single complex with a count rate equal to the sum of the constituent line rates. The heavy-lined triangles represent the principal UL x-ray peaks produced in the decay of Pu and the light-lined triangles represent the interference NpL x rays produced in the decay of ^{241}Am. The interference lines from natural soil are represented by dashed triangles. The rates shown are for Pu-Am activity of 1 pCi in 1 g of soil (a = 2.22 dpm/g). The natural soil activity was assumed[15,16] to be 0.6 pCi/g ^{232}Th and 0.6 pCi/g ^{238}U in equilibrium except for 8% escape of ^{222}Rn. A detector peak efficiency of $\eta = 1$ was taken. The soil mass attenuation coefficients (μ/ρ) used were 5.55, 2.85 and 1.76 cm^2/g at 13.5, 17 and 20 keV, respectively.

The count rate distribution expected from weapons material, Rocky Flats soil, and fallout, in which the ^{241}Am activity is less than 20%, is shown in Figs. 5 and 6. The UL_{β_1} line is seen to be nearly free from interference from ^{241}Am and from soil activity whereas the UL_{α_1} and UL_{γ_1} lines suffer from excessive interference and therefore are of very limited spectroscopic value at a 1 pCi level. One might note that UL x rays produced in the decay chain of ^{238}U interfere directly with those from Pu, however their effect is negligible at a level of ~1 pCi of Pu. We expect approximately 250 counts in a 10^3 min overnight run in the UL_{β_1} peak with the Si array of Fig. 2, which has a detection area of 50 cm^2. In the absence of excessive background continuum this would lead to a measurement uncertainty of less than 10%, which is considered adequate. Thus, when the relative abundance of ^{241}Am is low, it is apparently feasible to measure 1 pCi of Pu in 1 g of soil.

In reactor waste (Fig. 7) where the activity of ^{241}Am has built up over a period of 10 years to more than 60%, the NpL x rays obscure much of the UL_{α_1} and UL_{β_1} peaks, but not the UL_{γ_1} peak. However, the latter is largely overlapped by the $PaL_{\gamma_{2,3}}$ complex from soil. Since soil activity can vary from area to area by as much[16] as ±100%, the count rate in the UL_{γ_1} peak must be 10 times higher than that of the $PaL_{\gamma_{2,3}}$ peak for a 10% measurement uncertainty. Such a count rate would correspond to a minimum detectable activity of 8 pCi.

A figure of merit for the Si detector array can be obtained by comparing its sensitivity with that of a NaI phoswich. Although the capabilities of these two detectors are not the same, such a comparison may nevertheless be instructive. The poor energy resolution of NaI (FWHM ≈ 6 keV at 17 keV) precludes its use for elemental identification by L x-ray detection in the manner that Si detectors are used. However, if the identity of the element emitting the x rays is known, one could make a gross L x-ray measurement instead of measuring the individual lines, provided that the source activity level is well above the uncertainty in the background level. The average activity in soil due to the decay chains of ^{232}Th and ^{238}U is 0.6 pCi/g for each. Assuming area-to-area variations of ±100%, for a measurement uncertainty of 10%, the minimum detectable level corresponds to an x-ray intensity of 6 pCi of background activity. The combined intensity of ^{232}Th and ^{238}U is 130 x rays/100 α decays of each (Table I). The total L x-ray intensity from Pu-Am, for example in weapons material, is 7.5 x rays/100 α decays (Table IV). Thus, the minimum

Table IV

LINE INTENSITIES OF L X RAYS
EMITTED IN THE DECAY OF Pu AND Am

Energy (keV)	X-Ray Line	^{236}Pu	^{239}Pu	^{240}Pu	^{241}Am	Weapons Material	Rocky Flats Soil	Worldwide Fallout	Reactor Waste (aged)
		X Rays/100 α Decays							
11.62	UL_ℓ	0.31	0.10	0.25		0.12	0.13	0.13	0.11
11.89	NpL_ℓ				0.92	0.04	0.06	0.16	0.59
13.44	UL_{α_2}	0.52	0.17	0.43		0.22	0.22	0.23	0.18
13.61	UL_{α_1}	4.56	1.52	3.78		1.91	1.99	2.01	1.60
13.76	NpL_{α_2}				1.56	0.07	0.11	0.28	1.00
13.94	NpL_{α_1}				13.71	0.59	0.96	2.42	8.77
16.42	UL_{β_2}	0.94	0.31	0.78		0.39	0.41	0.42	0.33
16.57	UL_{β_4}	0.04	0.05	0.03		0.04	0.04	0.03	0.01
16.84	NpL_{β_2}				2.83	0.12	0.20	0.50	1.81
17.06	NpL_{β_4}				2.65	0.11	0.19	0.47	1.70
17.07	UL_{β_5}	0.19	0.06	0.16		0.08	0.08	0.08	0.07
17.22	UL_{β_1}	6.00	1.90	4.97		2.44	2.56	2.60	2.11
17.45	UL_{β_3}	0.04	0.05	0.03		0.04	0.04	0.03	0.01
17.51	NpL_{β_5}				0.57	0.02	0.04	0.10	0.36
17.75	NpL_{β_1}				9.56	0.41	0.67	1.69	6.12
17.99	NpL_{β_3}				2.42	0.10	0.17	0.43	1.55
20.16	UL_{γ_1}	1.33	0.42	1.10		0.54	0.56	0.57	0.47
20.49	UL_{γ_2}	0.01	0.01	0.01		0.01	0.01	0.01	--
20.72	UL_{γ_3}	0.01	0.01	0.01		0.01	0.01	0.01	--
20.79	NpL_{γ_1}				2.13	0.09	0.15	0.37	1.36
20.85	UL_{γ_6}	0.25	0.08	0.21		0.10	0.10	0.11	0.09
21.09	NpL_{γ_2}				0.71	0.03	0.05	0.13	0.45
21.33	NpL_{γ_3}				0.74	0.03	0.05	0.13	0.47
21.49	NpL_{γ_6}				0.40	0.02	0.03	0.07	0.26

detectable Pu activity with NaI is (6 x 130)/7.5 = 104 pCi. For the same case (Fig. 5) it was shown that the *minimum detectable activity with the Si array is 1 pCi.* The larger area of NaI detectors reduces the counting time required for a given statistical accuracy, but not the minimum detectable level. For a gross counting detector like NaI, the latter is determined mainly by the uncertainty in background activity.

VII. Conclusion

The minimum Pu concentration in soil that can be measured in the presence of natural background and ^{241}Am interference, by *L x-ray detection using an array of nine edge-mounted Si detectors, has been* evaluated. For contaminants such as worldwide fallout, weapons material, and Rocky Flats soil, in which the ^{241}Am activity is less than 20%, the minimum detectable Pu activity is expected to approach 1 pCi in 1 g of soil. This concentration is comparable to the natural activity in soil from the decay chains of ^{232}Th and ^{238}U. For comparison, the minimum detectable Pu activity with NaI detectors is 100 times higher.

For contaminants such as reactor waste (aged 10 yrs), in which the ^{241}Am activity is more than 60%, the natural activity from soil limits the minimum detectable Pu level at somewhat less than 10 pCi.

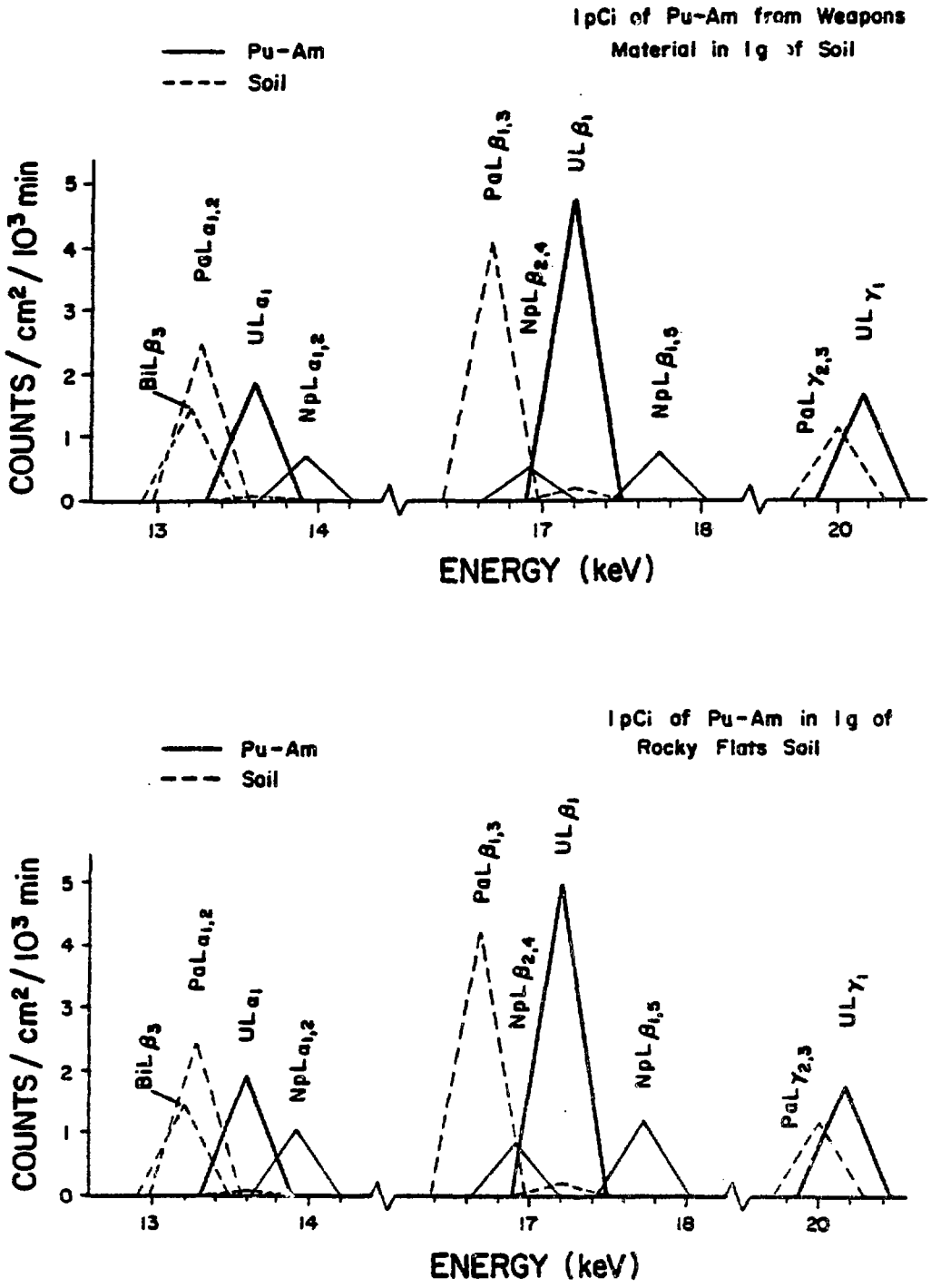

Fig. 5 Bar-type diagram showing expected detector count rates due to 1 pCi of Pu-Am from weapons material in 1 g of soil (top) and 1 pCi of Pu-Am in 1 g of Rocky Flats soil (bottom). UL x-ray peaks are from Pu decay and NpL x-ray peaks are from Am decay. UL_{β_1} line is nearly free from interference, making the measurement of 1 pCi of Pu appear feasible.

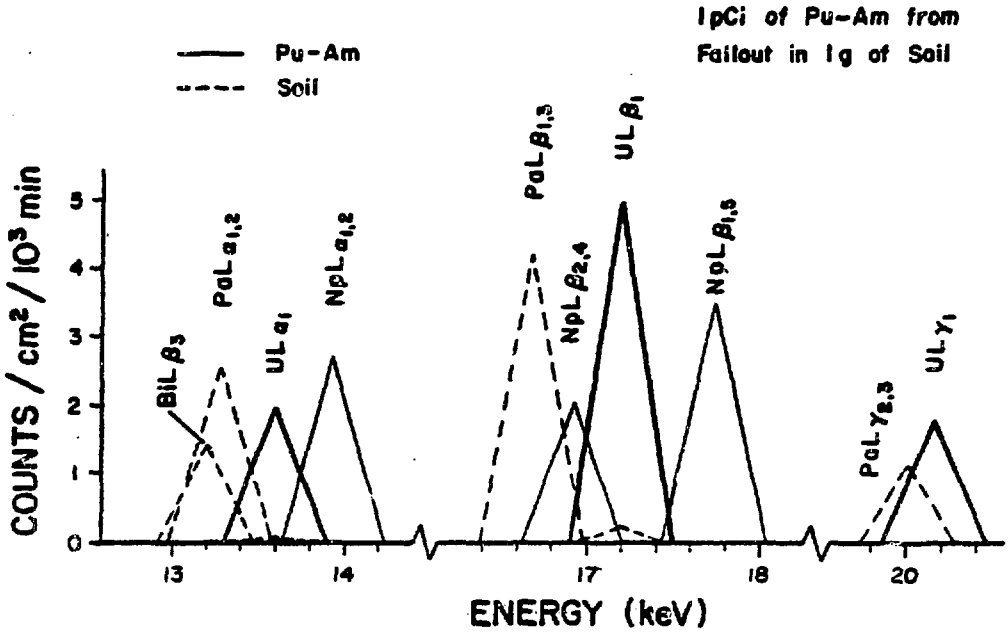

Fig. 6 Bar-type diagram showing expected detector count rates due to 1 pCi of Pu-Am from fallout in 1 g of soil. UL x-ray peaks are from Pu decay and NpL x-ray peaks are from Am decay. Although interference of $NpL_{\beta_{2,4}}$ line with UL_{β_1} is somewhat more pronounced than in Fig. 5, the measurement of 1 pCi of Pu still appears feasible.

Acknowledgment

Discussions with I. Ahmad and M. S. Freedman were most informative and instructive. The assistance of M. J. Cattelino in carefully carrying out lengthy computations is gratefully acknowledged.

References

1. P. M. C. Barretto: Radon-222 Emanation Characteristics of Rocks and Minerals. In Radon in Uranium Mining, IAEA, Vienna, 1975, pp. 129-150
2. D. G. Vasilik and R. W. Martin: $UL_{\alpha,\beta,\gamma}$ X-Ray Intensities from the Alpha Decay of ^{238}Pu. In Nucl. Instr. & Meth. 135, 405-406 (1976)
3. K. L. Swinth: A Solid State X-Ray Alpha Coincidence Counter. IEEE Trans. Nucl. Sci. NS-18, No. 1, 125 (1971)
4. J. W. Halley and D. Englekemeir: L Fluorescence Yields in Heavy Elements. Phys. Rev. 134, A24 (1964)
5. J. Byrne, W. Cielletly, M. A. S. Ross and F. Shaikh: L_2 - Subshell Yield Measurements in Pu^{240}, U^{236}, and U^{234}. Phys. Rev. 170, 170 (1968)
6. D. Newton: Interlaboratory Comparison of Techniques for Measuring Lung Burdens of Low Energy X-Ray Emitters. IAEA-R-1260-F (1974)
7. N. A. Coddington: Determination of the Ratio of L X-Rays to Alpha Particles Emitted by Pu-239. Air Force Weapons Laboratory Report AFWL-TR-69-82 (1969)
8. I. Ahmad: Nuclear Spectroscopic Studies of Some Very Heavy Odd-Mass Nuclides. Lawrence Radiation Laboratory, Report UCRL-16888 (1966)
9. H. I. Israel: Phys. Rev. 88, 682 (1952)
10. D. West and J. K. Dawson: Proc. Phys. Soc., London, 64A, 586 (1951)
11. J. L. Campbell and L. A. McNelles: Americium-241 as a Low-Energy Photon Intensity Standard. Nucl. Instr. & Meth. 17, 519-532 (1974)
12. Recommended Nuclear Data for Calibrated Solid Gamma Sources (IAEA, Vienna, 1969 and 1971)
13. R. J. Geherke and R. A. Lokken: Calibration of the Efficiency of a Si(Li) Photo Spectrometer in the Energy Region 5 to 125 keV. Nucl. Instr. & Meth. 97, 219-228 (1971)
14. H. L. Beck, J. E. McLaughlin and K. M. Miller: In Situ Determinations of Environmental Plutonium and its Related Nuclides. IEEE Trans. Nucl. Sci. NS-23, No. 1, 676-682 (1976)

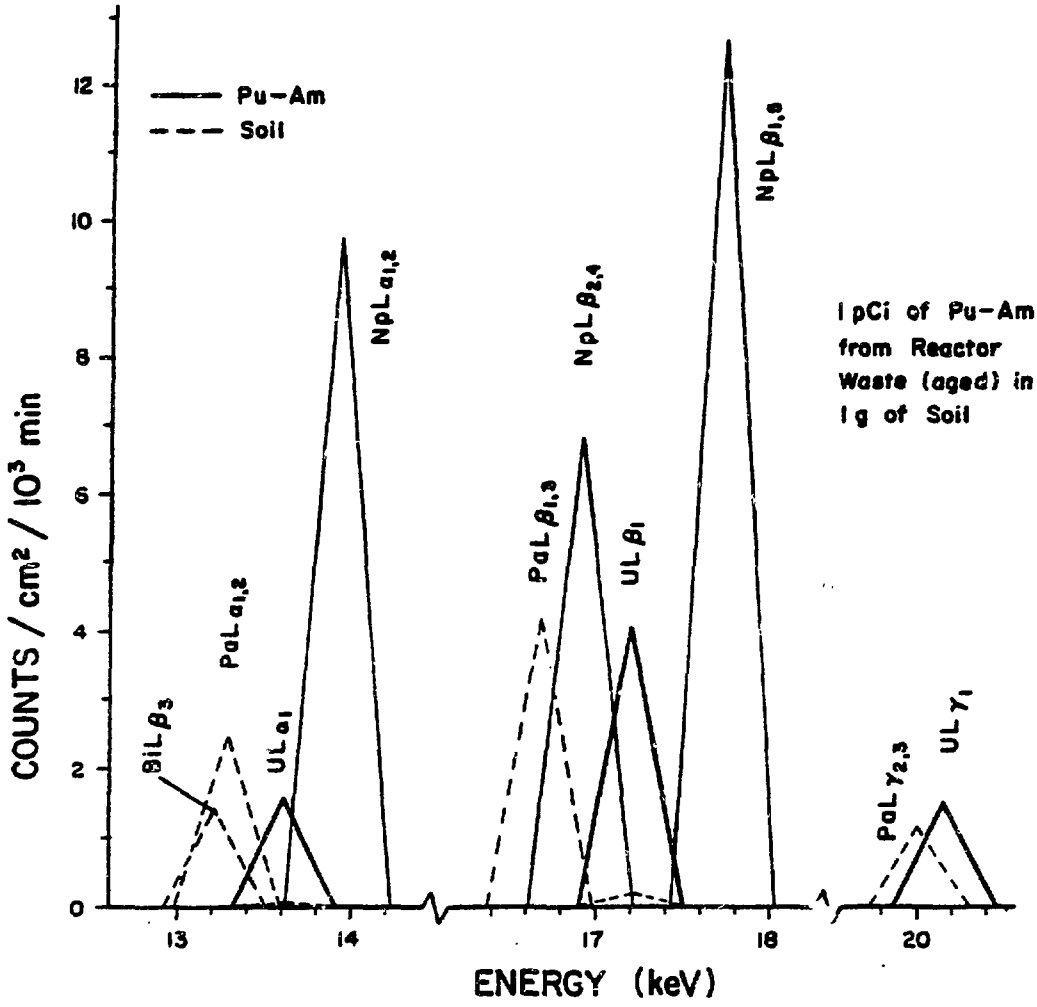

Fig. 7 Bar-type diagram showing expected detector count rates due to 1 pCi of Pu-Am from reactor waste in 1 g of soil. UL x-ray peaks are from Pu decay and NpL x-ray peaks are from Am decay. In 10 years ^{241}Am activity built up to more than 60%, producing intense NpL lines that obscure $UL\alpha_1$ and $UL\beta_1$ peaks. For Pu concentrations higher than 8 pCi/g, $UL\gamma_1$ line is sufficiently above background ($PaL\gamma_{2,3}$) to make meaningful measurements feasible.

15. L. R. Anspaugh, P. L. Phelps, P. H. Gudiksen, C. L. Lindeken and G. W. Huckabay: The In-Situ Measurement of Radionuclides in the Environment with a Ge(Li) Spectrometer. In The Natural Radiation Environment II, CONF-720805-P1, Houston, Texas, 1975, pp. 279-303

16. L. D. Stephens, A. R. Smith and R. H. Thomas: An Analytical Approach to Environmental Radiation Measurements. IEEE Trans. Nucl. Sci. NS-23, No. 1, 719-725 (1976)

17. Nuclear Data Sheets; compiled by K. Way et al. Printing and Publishing Office, National Academy of Sciences-National Research Council, Washington, D.C. 20025

18. Table of Isotopes (6th ed): C. M. Lederer, J. M. Hollander and I. Perlman. John Wiley & Sons, Inc., New York, 1967

19. W. Bambynek, B. Crasemann, R. W. Fink, H. U. Freund, H. Mark, C. D. Swift, R. E. Price and P. V. Rao: X-Ray Fluorescence Yields, Auger, and Coster-Kronig Transition Probabilities. Rev. Mod. Phys. 44, 719-721 (1972)

20. J. H. Scofield: Radiative Decay Rates of Vacancies in the K and L Shells. Phys. Rev. 179, 9 (1969)

21. R. W. Fink and P. V. Rao: Tables of Experimental Values of X-Ray Fluorescence and Coster-Kronig Yields for the K-, L- and M-Shells. In Handbook of Spectroscopy, J. W. Robinson, ed., CRC Press, Cleveland, Ohio, 1974, pp. 219-229

Appendix A

RADIATION INTENSITY PER UNIT AREA FROM A DISTRIBUTED SOURCE

The radiation intensity at the surface of a planar source in which the activity is distributed in an absorbing matrix, is presented here for an infinitely thick matrix in a single calculation and in a calculation by layers.

I. Intensity from an Infinitely Thick Source

Consider a differential layer of thickness dx having a radiation intensity per unit area $i_o dx$. The intensity per unit solid angle (fractional) that would be observed from this layer through an absorber of thickness x, having a linear attenuation coefficient μ is

$$\frac{di}{d\Omega}(\theta,x) = i_o\, e^{-\frac{\mu x}{\cos\theta}}\, dx \qquad (A1)$$

where θ is the angle of the photon path with respect to the normal direction. The intensity per unit solid angle $dI/d\Omega$ for a source of thickness x is obtained by integrating the differential intensity $di/d\Omega$ on x

$$\frac{dI}{d\Omega}(\theta) = i_o \int_0^{\infty} e^{-\frac{\mu x}{\cos\theta}}\, dx = I_n \cos\theta \qquad (A2)$$

where $I_n = i_o/\mu$ is the normal ($\theta = 0$) intensity per unit solid angle for an infinitely thick source.

The fractional solid angle can be expressed as $\Omega = (1-\cos\theta)/2$ and therefore

$$\cos\theta = 1-2\Omega. \qquad (A3)$$

The intensity per unit solid angle $dI/d\Omega$ is expressed as a function of the accumulated solid angle Ω by substituting Eq. (A3) in Eq. (A2)

$$\frac{dI}{d\theta}(\theta) = \frac{dI}{d\Omega}(\Omega) = I_n(1-2\Omega). \qquad (A4)$$

The total radiation intensity I_a per unit source area is obtained by integrating Eq. (A4) over half the solid angle

$$I_a = I_n \int_0^{0.5} (1-2\Omega)\, d\Omega = 0.25\, I_n. \qquad (A5)$$

One might note that Eq. (A4) is a line that with the axes forms a right angle triangle in which the height $dI/d\Omega = I_n$, the base $\Omega = 0.5$ and the total intensity is the area $I_a = 0.25\, I_n$.

II. Intensity from an Infinitely Thick Source by Layers

Consider an infinitely thick source divided into five layers of progressively increasing thickness so that each layer contributes 1/5 of the total normal intensity at the detector. Each layer is then represented by an equivalent point source. From Eqs. (8) and (9), the normal intensity per unit solid angle for the first layer is

$$0.2\, I_n = I_n(1 - e^{-\mu d_1}) \qquad (A6)$$

where d_1 is the thickness of layer I and $e^{-\mu d_1} = 0.8$. The intensity for the second layer is

$$0.2\, I_n = I_n(e^{-\mu d_1} - e^{-\mu d_2}) \qquad (A7)$$

where d_2-d_1 is the thickness of layer II and $e^{-\mu d_2} = 0.6$. Layers III-V follow a similar pattern.

Using linear interpolation, the average transmission of the point source representing layer I is 0.9 and that of layer II is 0.7. Thus the intensity in the normal direction per unit area solid angle from source I is

$$0.2\, I_n = I_1\, e^{-\mu x_1} = 0.9\, I_1 \qquad (A8)$$

where I_1 is the intensity at the source and x_1 is the distance of the source from the surface. The intensity per unit area solid angle from source I as a function of the angle θ, between the photon path and the normal, is

$$\frac{dI_1}{d\Omega}(\theta) = I_1\, e^{-\frac{\mu x_1}{\cos\theta}} = I_1(0.9)^{\frac{1}{\cos\theta}}. \qquad (A9)$$

Similarly, the intensity for source II is

$$\frac{dI_2}{d\Omega}(\theta) = I_2\, e^{-\frac{\mu x_2}{\cos\theta}} = I_2(0.7)^{\frac{1}{\cos\theta}}. \qquad (A10)$$

From Eq. (A3) we calculated the total fractional solid angle Ω as a function of θ and plotted $dI/d\Omega$ vs. Ω for layers I, III and V as shown in Fig. 3.

Appendix B

PROCEDURE FOR CALCULATING L X-RAY INTENSITIES

The L x-ray intensities were determined in two stages as presented here in outline form.

I. Total L X-Ray Intensity

Designations:

α: Internal conversion coefficient[17,18] (e/γ)

I_β: Branching intensity[17,18] (transitions/decay)

I_γ: Gamma intensity[17,18] (γ's/decay)

I_{eL}: L conversion-electron intensity (vacancies/decay)

I_{XL}: L x-ray intensity (x rays/decay)

$\bar{\omega}_L$: Mean L-shell fluorescent yield[19] (x rays/vacancy)

For any one transition:

$$I_\beta = I_\gamma + I_e$$

$$I_e = I_\gamma \alpha$$

$$I_\beta = I_\gamma (1+\alpha) = I_\gamma(1+\alpha_K+\alpha_L+\alpha_M)$$

$$I_{eL} = I_\gamma \alpha_L = I_\beta \frac{\alpha_L}{1+\alpha_K+\alpha_L+\alpha_M}$$

$$I_{XL} = I_{eL} \cdot \bar{\omega}_L$$

The total L x rays/α decay are equal to the sum of the I_{XL} intensities produced in all the deexcitation transitions of the decay.

When transitions in a given decay have different multipolarities, say, E2 and M1, then

$$I_{XL}(E2) = I_\gamma \cdot \alpha_L(E2) \cdot \bar{\omega}_L$$

$$I_{XL}(M1) = I_\gamma \cdot \alpha_L(M1) \cdot \bar{\omega}_L$$

where $\alpha_L(E2)$ and $\alpha_L(M1)$ are the conversion coefficients associated with the E2 and M1 transitions, respectively. For transitions of mixed multipolarity where, say, p go by E2 and 1-p go by M1, then

$$I_{XL}(E2) = I_\gamma \cdot p\ \alpha_L(E2) \cdot \bar{\omega}_L$$

$$I_{XL}(M1) = I_\gamma \cdot (1-p)\ \alpha_L(M1) \cdot \bar{\omega}_L$$

The total L x-ray intensity is always

$$I_{XL} = I_{XL}(E1)+I_{XL}(E2)+I_{XL}(M1)+\ldots.$$

Excited states with branching intensities of less than 1% were considered negligible provided all higher states could also be neglected.

II. X-Ray Line Intensity

Definitions:

N_{L_i}: Fraction of primary vacancies created in subshell i of shell L

$$N_{L_i} = \frac{\alpha_{L_i}}{\alpha_{L_1} + \alpha_{L_2} + \alpha_{L_3}}$$

where α_{L_i} is the conversion coefficient of subshell i of shell L.

N_{L_i} is a function of the multipolarity and energy of the transition creating the vacancies. The values used in the computations are given in Table B1.

$f_{L_iL_j}$: Coster-Kronig transition probability for shifting a vacancy from subshell L_i to subshell L_j.

The f values used in the computations are given in Table B2.

V_{L_i}: Fraction of vacancies created in subshell i of shell L including vacancies shifted by Coster-Kronig transitions. Thus, the vacancy distribution in the L subshells including those shifted by Coster-Kronig transitions are

$$V_{L_1} = N_{L_1}$$

$$V_{L_2} = N_{L_2} + f_{L_{12}} N_{L_1}$$

$$V_{L_3} = N_{L_3} + f_{L_{23}} N_{L_2} + (f_{L_{13}}+f_{L_{12}} f_{L_{23}}) N_{L_1}$$

ω_{L_i}: Fluorescent yield of subshell i of shell L. The ω_{L_i} values used in the computations are given in Table B3.

$V_{L_i}\ \omega_{L_i}$: Number of radiative transitions to subshell i per vacancy in L shell.

R_{L_i}: Fraction of radiative transitions to subshell i of shell L

$$R_{L_i} = \frac{V_{L_i}\ \omega_{L_i}}{V_{L_1}\ \omega_{L_1} + V_{L_2}\ \omega_{L_2} + V_{L_3}\ \omega_{L_3}}$$

$\Gamma_{W_jL_i}$: X-ray emission rate[20] resulting from filling a vacancy in subshell i of shell L by an electron from subshell j of shell W as a fraction of the total emission rate due to electron transitions from all higher shells to subshell i of shell L.

Y_{L_q}: Intensity of L_q x rays ($L\alpha_1$, $L\alpha_2$, $L\beta_1$ ...) as a fraction of the total L x rays.

$$Y_{L_q} = \Gamma_{W_jL_i} \cdot R_{L_i}$$

I_{XL_q}: Intensity of any L_q x-ray line

$$I_{XL_q} = I_{XL} \cdot Y_{L_q}$$

The radiative transition intensity R_{L_i} and in turn Y_{L_q} are unique functions of the multipolarity and the energy of the transition creating the L vacancies. When a given decay involves transitions of different multipolarities, say, E2 and M1, then

$$I_{XL_q}(E2) = I_{XL}(E2) \cdot Y_{L_q}(E2)$$

$$I_{XL_q}(M1) = I_{XL}(M1) \cdot Y_{L_q}(M1)$$

and the total L_q line intensity is

$$I_{XL_q} = I_{XL_q}(E2) + I_{XL_q}(M1)$$

where $Y_{L_q}(E2)$ and $Y_{L_q}(M1)$ are the relative L_q intensities associated with the E2 and M1 transitions, respectively. The values for $Y_{L_q}(E1)$, $Y_{L_q}(E2)$, and $Y_{L_q}(M1)$ used in the computations are given in Table B4.

Table B1

PRIMARY VACANCY DISTRIBUTION IN L SUBSHELLS
AS USED IN COMPUTATIONS

Transition Multipolarity	Z Range	N_{L_1}	N_{L_2}	N_{L_3}
E1	$86 \le Z \le 93$	0.36	0.31	0.33
E2	"	0.02	0.54	0.44
M1	"	0.89	0.10	0.01
M1	$81 \le Z \le 83$	0.90	0.09	0.01

Table B2

COSTER-KRONIG YIELDS
AS USED IN COMPUTATIONS

Z Range	f_{12}	f_{13}	f_{23}
$81 \le Z \le 83$	0.155†	0.56†	0.164†
$86 \le Z \le 93$	0.069*	0.575*	0.102*

†Ref. (21)
*Ref. (19)

Table B3

L SUBSHELL FLUORESCENT YIELDS[19]
AS USED IN COMPUTATIONS

Z Range	ω_{L_1}	ω_{L_2}	ω_{L_3}
$81 \le Z \le 83$	0.07	0.346	0.334
$86 \le Z \le 93$	0.2	0.485	0.446

Table B4

RELATIVE INTENSITIES OF L X-RAY LINES
AS USED IN COMPUTATIONS

X-Ray Line L_q	$Y_{L_q}(E1)$ $86 \le Z \le 93$	$Y_{L_q}(E2)$ $86 \le Z \le 93$	$Y_{L_q}(M1)$ $86 \le Z \le 93$	$Y_{L_q}(M1)$ $81 \le Z \le 83$
	Percent of Total L X Rays			
L_ℓ	2.37	2.09	2.20	2.30
L_{α_1}	35.25	31.05	32.73	39.54
L_{α_2}	4.01	3.54	3.73	4.48
L_{β_1}	25.41	40.80	12.07	19.24
L_{β_2}	7.27	6.41	6.75	7.53
L_{β_3}	4.66	0.26	11.35	7.22
L_{β_4}	5.10	0.28	12.41	6.48
L_{β_5}	1.47	1.29	1.36	0.93
L_{γ_1}	5.65	9.06	2.68	3.89
L_{γ_2}	1.36	0.08	3.32	1.66
L_{γ_3}	1.42	0.08	3.45	2.01
L_{γ_6}	1.05	1.69	0.50	0.45

Appendix C

SOURCE LIST OF LINE INTENSITIES OF L X RAYS
EMANATING FROM SOIL IN THE DECAY CHAINS OF ^{238}U AND ^{232}Th

Energy (keV)	X-Ray Line	Parent Decay	Decay Chain	Intensity†
8.95	TlL_ℓ	$^{212}Bi(\alpha)$	^{232}Th	0.20
9.42	BiL_ℓ	$^{214}Pb(\beta)$	^{238}U	0.13*
		$^{210}Pb(\beta)$	"	0. *
		$^{212}Pb(\beta)$	^{232}Th	0.05
10.13	RnL_ℓ	$^{226}Ra(\alpha)$	^{238}U	0.01
		$^{224}Ra(\alpha)$	^{232}Th	0.01
10.17	TlL_{α_2}	$^{212}Bi(\alpha)$	^{232}Th	0.39
10.27	TlL_{α_1}	$^{212}Bi(\alpha)$	^{232}Th	3.43
10.45	PbL_{α_2}	$^{208}Tl(\beta)$	^{232}Th	0.01
10.55	PbL_{α_1}	$^{208}Tl(\beta)$	^{232}Th	0.05
10.63	RaL_ℓ	$^{230}Th(\alpha)$	^{238}U	0.18
		$^{232}Th(\alpha)$	^{232}Th	0.18
		$^{228}Th(\alpha)$	"	0.20
10.73	BiL_{α_2}	$^{214}Pb(\beta)$	^{238}U	0.25*
		$^{210}Pb(\beta)$	"	1.11*
		$^{212}Pb(\beta)$	^{232}Th	0.11
10.84	BiL_{α_1}	$^{214}Pb(\beta)$	^{238}U	2.21*
		$^{210}Pb(\beta)$	^{238}U	9.78*
		$^{212}Pb(\beta)$	^{232}Th	0.99
11.12	ThL_ℓ	$^{238}U(\alpha)$	^{238}U	0.19
		$^{234}U(\alpha)$	"	0.23
		$^{228}Ac(\beta)$	^{232}Th	0.61
11.13	PoL_α	$^{214}Bi(\beta)$	^{238}U	0.03*
11.35	PaL_ℓ	$^{234}Th(\beta)$	^{238}U	0.25
11.60	RnL_{α_2}	$^{226}Ra(\alpha)$	^{238}U	0.02
		$^{224}Ra(\alpha)$	^{232}Th	0.01
11.62	UL_ℓ	$^{234m}Pa(\beta)$	^{238}U	0.01
11.72	RnL_{α_1}	$^{226}Ra(\alpha)$	^{238}U	0.14
		$^{224}Ra(\alpha)$	^{232}Th	0.09
11.93	TlL_{β_4}	$^{212}Bi(\alpha)$	^{232}Th	0.57
12.19	RaL_{α_2}	$^{230}Th(\alpha)$	^{238}U	0.31
		$^{232}Th(\alpha)$	^{232}Th	0.30
		$^{228}Th(\alpha)$	"	0.35
12.21	TlL_{β_1}	$^{212}Bi(\alpha)$	^{232}Th	1.67
12.27	TlL_{β_2}	$^{212}Bi(\alpha)$	^{232}Th	0.65
12.30	PbL_{β_4}	$^{208}Tl(\beta)$	^{232}Th	0.01
12.34	RaL_{α_1}	$^{230}Th(\alpha)$	^{238}U	2.70
		$^{232}Th(\alpha)$	^{232}Th	2.61
		$^{228}Th(\alpha)$	"	3.04
12.39	TlL_{β_3}	$^{212}Bi(\alpha)$	^{232}Th	0.63
12.62	PbL_{β_1}	$^{208}Tl(\beta)$	^{232}Th	0.04
12.62	PbL_{β_2}	$^{208}Tl(\beta)$	^{232}Th	0.01
12.64	TlL_{β_5}	$^{212}Bi(\alpha)$	^{232}Th	0.08
12.69	BiL_{β_4}	$^{214}Pb(\beta)$	^{238}U	0.36*
		$^{210}Pb(\beta)$	"	1.60*
		$^{212}Pb(\beta)$	^{232}Th	0.16
12.79	PbL_{β_3}	$^{208}Tl(\beta)$	^{232}Th	0.01
12.81	ThL_{α_2}	$^{238}U(\alpha)$	^{238}U	0.32
		$^{234}U(\alpha)$	"	0.39
		$^{228}Ac(\beta)$	^{232}Th	1.03
12.97	ThL_{α_1}	$^{238}U(\alpha)$	^{238}U	2.83
		$^{234}U(\alpha)$	"	3.42
		$^{228}Ac(\beta)$	^{232}Th	9.04
12.99	BiL_{β_2}	$^{214}Pb(\beta)$	^{238}U	0.42*
		$^{210}Pb(\beta)$	"	1.86*
		$^{212}Pb(\beta)$	^{232}U	0.18
13.02	BiL_{β_1}	$^{214}Pb(\beta)$	^{238}U	1.08*
		$^{210}Pb(\beta)$	"	4.76*
		$^{212}Pb(\beta)$	^{232}Th	0.48
13.12	PaL_{α_2}	$^{234}Th(\beta)$	^{238}U	0.43
13.21	BiL_{β_3}	$^{214}Pb(\beta)$	^{238}U	0.40*
		$^{210}Pb(\beta)$	"	1.79*
		$^{212}Pb(\beta)$	^{232}Th	0.18
13.29	PaL_{α_1}	$^{234}Th(\beta)$	^{238}U	3.77
13.34	PoL_{β_2}	$^{214}Bi(\beta)$	^{238}U	0.01*

Energy (keV)	X-Ray Line	Parent Decay	Decay Chain	Intensity†
13.39	$BiL\beta_5$	$^{214}Pb(\beta)$	^{238}U	0.05*
		$^{210}Pb(\beta)$	"	0.23
		$^{212}Pb(\beta)$	^{232}Th	0.02
13.44	$UL\alpha_2$	$^{234m}Pa(\beta)$	^{238}U	0.01
13.44	$PoL\beta_1$	$^{214}Bi(\beta)$	^{238}U	0.04*
13.61	$UL\alpha_1$	$^{234m}Pa(\beta)$	^{238}U	0.12
14.08	$RnL\beta_2$	$^{226}Ra(\alpha)$	^{238}U	0.03
		$^{224}Ra(\alpha)$	^{232}Th	0.02
14.29	$TlL\gamma_1$	$^{212}Bi(\alpha)$	^{232}Th	0.34
14.31	$RnL\beta_1$	$^{226}Ra(\alpha)$	^{238}U	0.18
		$^{224}Ra(\alpha)$	^{232}Th	0.11
14.57	$RnL\beta_5$	$^{226}Ra(\alpha)$	^{238}U	0.01
14.63	$TlL\gamma_2$	$^{212}Bi(\alpha)$	^{232}Th	0.14
14.68	$TlL\gamma_6$	$^{212}Bi(\alpha)$	^{232}Th	0.04
14.73	$TlL\gamma_3$	$^{212}Bi(\alpha)$	^{232}Th	0.17
14.76	$RaL\beta_4$	$^{230}Th(\alpha)$	^{238}U	0.02
		$^{232}Th(\alpha)$	^{232}Th	0.02
		$^{228}Th(\alpha)$	"	0.03
14.76	$PbL\gamma_1$	$^{208}Tl(\beta)$	^{232}Th	0.01
14.84	$RaL\beta_2$	$^{230}Th(\alpha)$	^{238}U	0.56
		$^{232}Th(\alpha)$	^{232}Th	0.54
		$^{228}Th(\alpha)$	"	0.63
15.23	$RaL\beta_1$	$^{230}Th(\alpha)$	^{238}U	3.55
		$^{232}Th(\alpha)$	^{232}Th	3.43
		$^{228}Th(\alpha)$	"	4.00
15.24	$BiL\gamma_1$	$^{214}Pb(\beta)$	^{238}U	0.22*
		$^{210}Pb(\beta)$	"	0.96*
		$^{212}Pb(\beta)$	^{232}Th	0.10
15.39	$RaL\beta_5$	$^{230}Th(\alpha)$	^{238}U	0.11
		$^{232}Th(\alpha)$	^{232}Th	0.11
		$^{228}Th(\alpha)$	"	0.13
15.55	$RaL\beta_3$	$^{230}Th(\alpha)$	^{238}U	0.02
		$^{232}Th(\alpha)$	^{232}Th	0.02
		$^{228}Th(\alpha)$	"	0.03
15.58	$BiL\gamma_2$	$^{214}Pb(\beta)$	^{238}U	0.09*
		$^{210}Pb(\beta)$	"	0.41*
		$^{212}Pb(\beta)$	^{232}Th	0.04
15.62	$ThL\beta_2$	$^{238}U(\alpha)$	^{238}U	0.58
		$^{234}U(\alpha)$	"	0.71
		$^{228}Ac(\beta)$	^{232}Th	1.87
15.64	$ThL\beta_4$	$^{238}U(\alpha)$	^{238}U	0.03
		$^{234}U(\alpha)$	"	0.03
		$^{228}Ac(\beta)$	^{232}Th	0.06
15.69	$BiL\gamma_6$	$^{214}Pb(\beta)$	^{238}U	0.03*
		$^{210}Pb(\beta)$	"	0.11*
		$^{212}Pb(\beta)$	^{232}Th	0.01
15.71	$BiL\gamma_3$	$^{214}Pb(\beta)$	^{238}U	0.11*
		$^{210}Pb(\beta)$	"	0.50*
		$^{212}Pb(\beta)$	^{232}Th	0.05
15.74	$PoL\gamma_1$	$^{214}Bi(\beta)$	^{238}U	0.01*
16.02	$PaL\beta_2$	$^{234}Th(\beta)$	^{238}U	0.78
16.10	$PaL\beta_4$	$^{234}Th(\beta)$	^{238}U	0.96
16.20	$ThL\beta_1$	$^{238}U(\alpha)$	^{238}U	3.71
		$^{234}U(\alpha)$	"	4.49
		$^{228}Ac(\beta)$	^{232}Th	11.87
16.21	$ThL\beta_5$	$^{238}U(\alpha)$	^{238}U	0.12
		$^{234}U(\alpha)$	"	0.14
		$^{228}Ac(\beta)$	^{232}Th	0.38
16.42	$UL\beta_2$	$^{234m}Pa(\beta)$	^{238}U	0.03
16.43	$ThL\beta_3$	$^{238}U(\alpha)$	^{238}U	0.02
		$^{234}U(\alpha)$	"	0.03
		$^{228}Ac(\beta)$	^{232}Th	0.08
16.63	$PaL\beta_5$	$^{234}Th(\beta)$	^{238}U	0.16
16.70	$PaL\beta_1$	$^{234}Th(\beta)$	^{238}U	2.50
16.77	$RnL\gamma_1$	$^{226}Ra(\alpha)$	^{238}U	0.04
		$^{224}Ra(\alpha)$	^{232}Th	0.03
16.93	$PaL\beta_3$	$^{234}Th(\beta)$	^{238}U	0.88
17.07	$UL\beta_5$	$^{234m}Pa(\beta)$	^{238}U	0.01

Energy (keV)	X-Ray Line	Parent Decay	Decay Chain	Intensity†
17.22	UL_{β_1}	$^{234m}Pa(\beta)$	^{238}U	0.16
17.29	RnL_{γ_6}	$^{226}Ra(\alpha)$	^{238}U	0.01
17.84	RaL_{γ_1}	$^{230}Th(\alpha)$	^{238}U	0.79
		$^{232}Th(\alpha)$	^{232}Th	0.76
		$^{228}Th(\alpha)$	"	0.89
18.19	RaL_{γ_2}	$^{230}Th(\alpha)$	^{238}U	0.01
		$^{232}Th(\alpha)$	^{232}Th	0.01
		$^{228}Th(\alpha)$	"	0.01
18.36	RaL_{γ_3}	$^{230}Th(\alpha)$	^{238}U	0.01
		$^{232}Th(\alpha)$	^{232}Th	0.01
		$^{228}Th(\alpha)$	"	0.01
18.42	RaL_{γ_6}	$^{230}Th(\alpha)$	^{238}U	0.15
		$^{232}Th(\alpha)$	^{232}Th	0.14
		$^{228}Th(\alpha)$	"	0.17
18.98	ThL_{γ_1}	$^{238}U(\alpha)$	^{238}U	0.82
		$^{234}U(\alpha)$	"	1.00
		$^{228}Ac(\beta)$	^{232}Th	2.64
19.31	ThL_{γ_2}	$^{238}U(\alpha)$	^{238}U	0.01
		$^{234}U(\alpha)$	"	0.01
		$^{228}Ac(\beta)$	^{232}Th	0.02
19.51	ThL_{γ_3}	$^{238}U(\alpha)$	^{238}U	0.01
		$^{234}U(\alpha)$	"	0.01
		$^{228}Ac(\beta)$	^{232}Th	0.02
19.56	PaL_{γ_1}	$^{234}Th(\beta)$	^{238}U	0.55
19.60	ThL_{γ_6}	$^{238}U(\alpha)$	^{238}U	0.15
		$^{234}U(\alpha)$	"	0.19
		$^{228}Ac(\beta)$	^{232}Th	0.49
19.90	PaL_{γ_2}	$^{234}Th(\beta)$	^{238}U	0.26
20.09	PaL_{γ_3}	$^{234}Th(\beta)$	^{238}U	0.27
20.16	UL_{γ_1}	$^{234m}Pa(\beta)$	^{238}U	0.04
20.22	PaL_{γ_6}	$^{234}Th(\beta)$	^{238}U	0.10
20.85	UL_{γ_6}	$^{234m}Pa(\beta)$	^{238}U	0.01

†X rays per 100 ^{238}U α decays or 100 ^{232}Th α decays.

*8% escape of ^{222}Rn from soil was assumed.